

Graph-Variate Signal Analysis

Keith Smith^{1,2,*}, Loukianos Spyrou¹, *Member, IEEE*, & Javier Escudero¹, *Member, IEEE*

Abstract—Incorporating graph-based techniques in the analysis of multivariate signals is becoming a standard method to understand the interdependency of activity recorded at different sites. The new research frontier in this field includes the important problem of how to assess dynamic changes of signal activity. We address this problem in a novel way by defining the *graph-variate signal* through the unified framework of multivariate signals and network science. Inspired by ideas in graph signal processing, we go in a new direction by considering the relationship between graph edges and the instantaneous graph signal, leveraging graphs of reliable connectivity information to filter instantaneous bivariate functions of the multivariate signal. This opens up a powerful and robust approach to analyse joint signal and network dynamics at sample resolution. Furthermore, this can be formulated as instantaneous networks for which standard network analysis can be implemented. In the case for which graph connectivity is estimated from the multivariate signal itself, we illustrate how the appropriate consideration of instantaneous graph signal functions allow for a novel dynamic connectivity measure, here referred to as *graph-variate dynamic (GVD) connectivity*, robust to spurious short-term dependencies. Particularly, we present appropriate functions for three pertinent connectivity metrics- correlation, coherence and the phase-lag index. Our approach can determine signals with a single correlated couple against wholly uncorrelated data up to 128 nodes in signal size; it is shown to be more robust than other GSP approaches in detecting a randomly traveling spheroid on a 3D grid and than standard dynamic connectivity in determining differences in EEG resting-state and task related activity, and we demonstrate its use in revealing hidden depth correlations from geographical gamma ray data.

I. INTRODUCTION

Network science provides a well tried and tested framework for analysing topologies of weighted edges derived from pairwise dependencies between the agents, recordings or information received at different points of a given space [1], [2]. An interesting case arises when graphs are constructed for the analysis of multivariate signals, where there is activity associated to individual nodes of the graph. Notably, the recently developed theory of Graph Signal Processing (GSP) [3], [4] outlines a promising approach to tackle such scenarios. In this setting, a signal, whose samples occur at graph nodes, is processed over the graph topology.

GSP is mainly concerned with the development of a cohesive signal processing theory for graph signals, analogous to classical signal processing [3]. Spectral graph techniques are implemented, using the Eigen-decomposition of either the graph adjacency matrix [4] or its Laplacian [3], to process

graph signals in a method called the Graph Fourier transform which has been applied in topics such as big data [5] and neuroscience [6]. Recent work on the integration of the temporal domain within the GSP framework is also underway [7], [8]. This spectral approach, however, presents hurdles in interpretation in light of the fact that the frequencies of the graph signal emerge through graph eigenvectors which relate to a still unquantified extent to the graph topology. Further, the graph signal itself remains a passive component in the analysis treated as a vector separate from the graph adjacency matrix.

On the other hand, the Dirichlet energy of a graph signal [3] defined as

$$\mathbf{x}^T \mathbf{L} \mathbf{x} = \sum_{i,j=1}^n w_{ij} (x_i - x_j)^2 \quad (1)$$

for graph weights w_{ij} and graph signal \mathbf{x} , where \mathbf{L} is the graph Laplacian, is a more directly extracted feature which has recently been considered to measure dynamic connectivity of brain function from EEG recordings [9]. This article considered a graph of pairwise signal correlations as a support for graph signals of instantaneous EEG activity, describing how the relationship between the Pearson correlation coefficient and the squared difference of the graph signals, the two components of (1) in this instance, complemented each other to provide a useful dynamic connectivity measure.

Although this already begins to radically reconsider how the Dirichlet energy can be treated, we will show that the true potential of this technique is limited in the classical GSP framework where one deals with graph adjacency matrices (or the Laplacian) and graph signal vectors and their matrix multiplications. Therefore, we construct a more flexible unified analytical framework for multivariate signals and graphs in which we frame new modes of analysis. These include generalising dynamic connectivity estimation for various different connectivity measures and a form of network analysis conducted at sample resolution of the multivariate signal.

The former is particularly timely and promising in light of new efforts required for estimating dynamic connectivity from multivariate signals. A large contingent of research solutions for temporal networks take the form of events occurring at edges (i.e. between two nodes) which change over time, geared towards data in which node specific activity is either not available or not meaningful [10]. Such outputs are also well suited to multi-layered network analysis [11]. For multivariate signals on the other hand, each component is directly associated with a node and often the signals are that from which the graph itself is constructed via pairwise signal correlations or dependencies. Nonetheless initial attempts have done well to devise temporal and multi-layer network methods to analyse multivariate signals.

¹Institute for Digital Communications, School of Engineering, University of Edinburgh, West Mains Rd, Edinburgh, EH9 3FB, UK

²Alzheimer Scotland Dementia Research Centre, Psychology Department, University of Edinburgh, 7 George Square, Edinburgh, EH8 9JZ, UK

*PhD funded by EPSRC, e-mail: k.smith@ed.ac.uk

In neuroimaging, for example, where activity is often recorded at sensors (MEG/EEG) or voxels (fMRI) and topological dependencies estimated via time-series correlations or phase dependencies, suitable methods for the temporal analysis of networks is an important open topic [12], [13]. Most recent studies go the route of implementing disjoint [14] or overlapping [15]–[17] windows to construct a number of distinct chronologically separated graphs to gain a foothold on changing connectivity patterns. This approach, however, is limited by the length of the window- the less samples used to define the network, the less reliable is the connectivity estimate. Fig. 1(a) illustrates this, showing independent realisations of an autoregressive process in which spurious strong correlations can be found in short windows. On the other hand, the larger the window used the less meaningful it is at determining temporally refined connectivity estimation. Therefore obtaining reliable transient information is difficult.

Though one may consider instantaneous phases alone [18] which do allow signal resolution analysis, they are wide open to spurious connections, Fig. 1 (a), and noisy fluctuations in the signal. Instead, we propose an elegant and flexible approach via graph-variate signal analysis named graph-variate dynamic (GVD) connectivity. Of particular benefit, this temporal analysis can be conducted up to the temporal resolution of the original signal and seeks to cancel spurious short-term effects by weighting analysis with stable graph dependencies which emphasises transient signal dynamics at the strongest connections and suppresses those from weak connections, illustrated in Fig 1(b), where transient activity common to i and j should be regarded with more credence than if it were between k and either i or j . Importantly, we provide a general framework for computing GVD connectivity and we provide reasonable solutions for amplitude, power and phase-based connectivity in the form of the correlation coefficient, coherence and phase-lag index, respectively.

We then demonstrate the power of our methodology by determining its ability to correctly identify the presence of correlations from various sizes of multivariate signals generated from an autoregressive process from which only a single couple of correlated signals exists. Furthermore, we demonstrate how the more refined analyses enabled by our generalisation provides greater accuracy in a simple randomly travelling spheroid detection problem than comparable approaches. Moreover, we show that our approach outperforms state-of-the-art dynamic connectivity methods in an EEG resting state paradigm and how our methods can be used as an investigative tool in geophysical exploration.

Our main aims are to introduce the general theoretical setting for graph-variate signal analysis (sections II & III) and to provide evidence for the benefits of the applications of this theory over comparable benchmark approaches in simulations and applications (section IV). We focus on taking a breadth first exploration of the possibilities encompassed by our framework since our methods are geared to answering, jointly, what are the stable connections in the data and how the data behave instantaneously, which are, til, now usually sought separately.

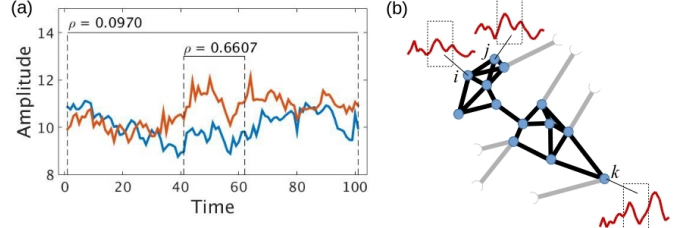


Fig. 1. (a) Specific example of spurious short-term correlation coefficient, ρ , from independent realisations of an autoregressive model. (b) Illustration of how long-term connectivity weighting (black edges connecting blue nodes) improves robustness of analysis of short-term transient dynamics. Nodes i , j and k all exhibit similar behaviour in the windowed epoch. However, from the topology of long-term connectivity it is clear that the correlation between i and j , with a shortest path of 1, is more meaningful whereas correlations between i/j and k , with shortest paths of 6, are likely spurious and should be disregarded.

II. GRAPH-VARIATE SIGNALS

The framework is initialised with the introduction of a graph-variate signal which includes a multivariate signal associated with the node set similarly to how graph definitions usually include the weighted adjacency matrix associated with the edge set. Through this definition, one provides an object unifying multivariate signals and network science.

Definition 1. We define the object $\Gamma = (\mathcal{V}, \mathbf{X}, \mathcal{E}, \mathbf{W})$ as a graph-variate signal where \mathcal{V} is the set of vertices with $|\mathcal{V}| = n$; $\mathbf{X} \in \mathbb{R}^{n \times p}$ the multivariate signal indexed by \mathcal{V} ; $\mathcal{E} = \{(i, j) : i, j \in \mathcal{V}\}$ the set of edges with $|\mathcal{E}| = 2m$; and $\mathbf{W} = \{w_{ij}\}_{(i,j) \in \mathcal{E}} \in \mathbb{R}^{n \times n}$ the weighted adjacency matrix encoding a relevant topology in which the multivariate signal is set. Then

- $(\mathcal{V}, \mathbf{X})$ is the node space composed of a matrix \mathbf{X} whose first dimension is indexed by the node set \mathcal{V} and second dimension is indexed by a sequential characteristic of activity at the nodes, typically time.
- $(\mathcal{E}, \mathbf{W})$ is the edge space composed of a weighted matrix \mathbf{W} indexed by the edge set \mathcal{E} .
- Γ constitutes the graph space of the combined node and edge spaces where vertices and edges joining those vertices are determined by the node labels $\{1, \dots, n\}$.

The node space, being that which contains the activity at the nodes, frames the standard analysis of multivariate signals. Indeed, this is formalised by a general node space function, $F_{\mathcal{V}}$, defined on the node space $(\mathcal{V}, \mathbf{X})$ as

$$\begin{aligned} F_{\mathcal{V}} : \mathbb{R}^{n \times p} &\rightarrow \mathbb{R}^{m \times q} \\ \mathbf{X} &\mapsto F_{\mathcal{V}}(\mathbf{X}), \end{aligned} \quad (2)$$

and, when applied in a single instance to pairs of channels at sample s , as

$$\begin{aligned} F_{\mathcal{V}} : \mathbb{R}^{2 \times 1} &\rightarrow \mathbb{R} \\ [x_i(s), x_j(s)]^T &\mapsto F_{\mathcal{V}}(x_i(s), x_j(s)). \end{aligned} \quad (3)$$

Useful examples of such functions where $n = m$ and $p = q$ include weight thresholds and a spectral filtering function, e.g. for bandpassing the signal in a frequency band of interest.

The edge space, on the other hand, is a topological space whose elements are the unlabeled isomorphism classes of

graphs of size n . This is where one finds the standard analysis of networks. A function $F_{\mathcal{E}}$ on the edge space $(\mathcal{E}, \mathbf{W})$ is defined on $\mathbb{R}^{n \times n}$ as

$$\begin{aligned} F_{\mathcal{E}} : \mathbb{R}^{n \times n} &\rightarrow \mathbb{R}^{m \times l} \\ \mathbf{W} &\mapsto F_{\mathcal{E}}(\mathbf{W}). \end{aligned} \quad (4)$$

Such functions can be thresholding when $n = m = l$, global network indices, such as transitivity or characteristic path length, when $m = l = 1$ and local network indices, such as the local clustering coefficient or betweenness centrality, when $m = n$ and $l = 1$. These are necessarily all invariants under graph isomorphisms- individuality of nodes is not considered.

The following definitions will be useful for specificity in the rest of this section.

Definition 2. An edge dimension preserving function, $\bar{F}_{\mathcal{E}}$, maps the adjacency matrix, $\mathbf{W} \in \mathbb{R}^{n \times n}$, to a new matrix $\tilde{\mathbf{W}} \in \mathbb{R}^{n \times n}$.

Definition 3. A node dimension preserving function, $\bar{F}_{\mathcal{V}}$, maps the multivariate signal, $\mathbf{X} \in \mathbb{R}^{n \times p}$, to a new signal $\tilde{\mathbf{X}} \in \mathbb{R}^{n \times p}$.

A key distinction to make here is that in this framework the signals are sampled with respect to a sequential characteristic, such as time, but the interdependencies are known or estimated and encoded in a graph topology, whereas in GSP the signal is sampled and thus processed over a graph topology. By theoretical considerations we will demonstrate that the former is more flexible for analysing multivariate signals.

We shall now consider how node and edge spaces can be combined to produce meaningful analyses for the graph-based analysis of multivariate signals. Important considerations of such operations pertain to how edge space operations can act on the node space and, reciprocally, how node space operations can act on the edge space. In the usual graph sense it is required that these operations preserve the inner dimensions whose size is the same as the node set, n , before acting on their reciprocal space.

A. Edge-dependent operations acting on the node space

Since the inner-dimensions of the edge space and node space agree, the output of any edge-dimension preserving function together with the usual matrix multiplication, \cdot , provide useful operations which act on the node space, $(\mathcal{V}, \tilde{\mathbf{X}})$:

$$\begin{aligned} \bar{F}_{\mathcal{E}}(\mathbf{W}) \cdot : \mathbb{R}^{n \times p} &\rightarrow \mathbb{R}^{n \times p} \\ \mathbf{X} &\mapsto \bar{F}_{\mathcal{E}}(\mathbf{W}) \cdot \mathbf{X}. \end{aligned} \quad (5)$$

We thus realise that $\bar{F}_{\mathcal{E}}(\mathbf{W}) \cdot$ is in fact a node dimension preserving function. Some of the simplest examples include the weighted adjacency matrix, \mathbf{W} , and the graph Laplacian, \mathbf{L} . Indeed, this property is exploited to formulate the various aspects of GSP where important definitions involve pre-matrix multiplication of the graph signal by matrices derived from graphs. For example, the GFT treats the eigenvectors of the Laplacian or the graph adjacency matrix as a basis for the decomposition of graph signals into graph frequency components. The l th eigenvector produces the l th frequency component of the graph signal, $\mathbf{x} \in \mathbb{R}^{n \times 1}$, defined as

$\mathbf{u}_l \cdot \mathbf{x}$. Similarly, graph convolution, translation, modulation and graph wavelets can be formulated as matrix multiplication on linear components of the graph signal. Further, polynomials of the adjacency and Laplacian matrices are implemented to construct graph signal filters in GSP in [4] and [3], respectively, which are then matrix multiplied by the graph signal. We will now evolve a new analysis of graph-variate signals by reciprocally considering node space functions acting on adjacency matrices.

B. Node-dependent operations acting on the edge space

Because the edge space is composed of pairs of elements in the node space, when combining the output of node space functions with the adjacency matrix it is most sensible to impose that the elements acting on the weight w_{ij} be bivariate functions of the signal at nodes i and j . In this manner, we define graph-variate signal analysis.

Definition 4. Graph-variate signal analysis is an all-to-all bivariate analysis of the signal \mathbf{X} weighted by the corresponding adjacency matrix \mathbf{W} .

Graph-variate signal analysis is facilitate by formulating a tensor, $\underline{\mathbf{J}} \in \mathbb{R}^{n \times n \times p}$, which is the output of a node space function defined as

$$J_{ijt} = \begin{cases} F_{\mathcal{V}}(x_i(t), x_j(t)), & i \neq j \\ 0, & i = j, \end{cases} \quad (6)$$

for some node space function $F_{\mathcal{V}}$.

In order to fully encode the graph-variability we consider both the edge and node spaces,

$$(\mathbf{W} \circ \underline{\mathbf{J}}_{(t)})_{ij} = \begin{cases} w_{ij} F_{\mathcal{V}}(x_i(t), x_j(t)), & i \neq j \\ 0, & i = j, \end{cases} \quad (7)$$

where $\underline{\mathbf{J}}_{(t)}$ denotes the t th $n \times n$ matrix of $\underline{\mathbf{J}}$ and \circ is the mode- k Hadamard product. This way w_{ij} , which encodes the relationship between nodes i and j , is multiplied by the relevant node space function on x_i and x_j .

It is also useful to define a new operator which allows node space operations to act on the edge space to provide local graph-variate analysis for each node.

Definition 5. For a matrix $\mathbf{A} \in \mathbb{R}^{n \times n}$ and 3D tensor $\underline{\mathbf{B}} \in \mathbb{R}^{n \times n \times p}$, composed of the p $n \times n$ matrices $\{\mathbf{B}_{(k)}\}_{k=1}^p$, their **signal product**, $\mathbf{A} \diamond \underline{\mathbf{B}}$, is matrix whose k th column is the vector $[\sum_j A_{ij} B_{jik}]_{i=1}^n$, which is the dot product of the i th rows of \mathbf{A} and the i th columns of $\mathbf{B}_{(k)}$.

Then

$$(\mathbf{W} \diamond \underline{\mathbf{J}})_{it} = \sum_{j=1}^n w_{ij} F_{\mathcal{V}}(x_i(t), x_j(t)). \quad (8)$$

A special case of this is GSP's node gradient formula [3] where $F_{\mathcal{V}}(x_i(t), x_j(t)) = (x_i(t) - x_j(t))^2$.

This operator has the interesting property of providing a reciprocal approach (up to linear combinations) for the matrix multiplication operator which allows edge space operations to act on the node space. From this, the limitations of the GSP framework for our ends are made most apparent. It is

straightforward to note that node space functions $x_j(t)$ and $\bar{x}_i(t) - x_j(t)$ are solutions for F_V in (8) to the equations $\mathbf{W} \diamond \mathbf{J} = \mathbf{W} \cdot \mathbf{X}$ and $\mathbf{W} \diamond \mathbf{J} = \mathbf{L} \cdot \mathbf{X}$, respectively. The limitations of adjacency matrix multiplication with signal vectors are revealed in the following.

Proposition 1. *For the output of an edge dimension preserving function $\bar{F}_E(\mathbf{W})$ and of a node dimension preserving function $\bar{F}_V(\mathbf{X})$,*

$$\bar{F}_E(\mathbf{W}) \cdot \mathbf{X} = \mathbf{W} \diamond \bar{F}_V(\mathbf{X}) \quad (9)$$

if and only if $\bar{F}_V(\mathbf{X}) = a_{ij}x_i(t) + a_{ji}x_j(t)$ for some constants $a_{ij}, a_{ji} \in \mathbb{R}$, and

$$\bar{F}_E(\mathbf{W}) = \begin{bmatrix} \sum_j a_{1j}w_{1j} & a_{21}w_{12} & \dots & a_{n1}w_{1n} \\ a_{12}w_{21} & \sum_j a_{2j}w_{2j} & \dots & a_{n2}w_{2n} \\ \vdots & \vdots & \ddots & \vdots \\ a_{1n}w_{n1} & a_{2n}w_{n2} & \dots & \sum_j a_{nj}w_{nj} \end{bmatrix}. \quad (10)$$

Proof. We first note that matrix multiplication with \mathbf{X} is linear on the entries of \mathbf{X} thus we cannot consider equating $\bar{F}_E(\mathbf{W}) \cdot \mathbf{X}$ to a graph weighted non-linear node space function- one cannot obtain elements $x_i(t)^p$ for $p > 1$. Further, since each element of $\bar{F}_E(\mathbf{W})$ is multiplied by an element of \mathbf{X} and each element of $\bar{F}_E(\mathbf{W})$ is multiplied by an entry of \mathbf{W} , there can be no constants in either function.

Now, in the linear case without constants for $\mathbf{x} \in \mathbb{R}^{n \times 1}$,

$$\begin{aligned} (\widetilde{\mathbf{W}} \cdot \mathbf{X})_{ti} &= \sum_{j=1}^n w_{ij}(a_{ij}x_i(t) + a_{ji}x_j(t)) \\ \iff \widetilde{w}_{ij} &= \begin{cases} \sum_{p=1}^n a_{ip}w_{ip} & i = j \\ a_{ji}w_{ij} & i \neq j, \end{cases} \end{aligned} \quad (11)$$

for coefficients $a_{ij} \in \mathbb{R}$, satisfying the proposition. \square

C. Graph-variate networks

Interestingly, from (7) we note that $\underline{\Delta}_{(t)} = \mathbf{W} \circ \mathbf{J}_{(t)}$ itself takes on a weighted adjacency matrix form and thus the tensor $\underline{\Delta} \in \mathbb{R}^{n \times n \times p}$ is a multi-layer network of sequentially related graphs. This is useful as we can then explore topological characteristics of a graph-variate signal at every sample. In classical network science, there are many methods proposed to analyse the topology of a graph by applying operations in the edge space, that is, on the edge weight matrix, \mathbf{W} . Such methods provide important insights and classifications of the interdependent relationships of the underlying objects [1]. In our experiments, we will implement a simple example of a local clustering coefficient, C_{loc} , of node i at time t , defined for the graph-variate signal as

$$C_{loc}(i, t) = \sum_{j,k=1}^n \Delta_{ijt} \Delta_{ikt} \Delta_{jkt} = (\underline{\Delta}_{(t)}^3)_{ii}. \quad (12)$$

Implementing network science on Δ could, for example, provide insights into rapid fluctuations in the topological relationships of the signals or, as we will focus on in section IV.B, could be used to develop techniques based jointly on pairwise signal dependencies and their spatial distances.

III. GRAPH-VARIATE DYNAMIC CONNECTIVITY ANALYSIS

Now we turn our attention to the special case in which the graph weights encode pairwise dependencies which have been estimated using the whole multivariate signal itself. Specifically, for important connectivity measures, we demonstrate how appropriate consideration of the node space function in graph-variate signal analysis provides a sample resolution analysis of dynamic connectivity. The following makes use of the instantaneous amplitude and phase components of the analytic representation of the univariate signals \mathbf{x}_i , of \mathbf{X} , $x_i^a(t) = s_i^a(t)e^{j\phi_i(t)}$.

We define a function of connectivity of pairwise channels, $\{\mathbf{x}_i, \mathbf{x}_j\}$, in \mathbf{X} as

$$H_V : \begin{matrix} \mathbb{R}^{2 \times p} \\ \{\mathbf{x}_i, \mathbf{x}_j\} \end{matrix} \rightarrow \begin{matrix} \mathbb{R} \\ H_V(\mathbf{x}_i, \mathbf{x}_j), \end{matrix} \quad (13)$$

where H_V is a node function of the entire signals \mathbf{x}_i and \mathbf{x}_j and $H_V(\mathbf{X}) = \mathbf{C} \in \mathbb{R}^{n \times n}$ such that

$$c_{ij} = \begin{cases} H_V(\mathbf{x}_i, \mathbf{x}_j), & i \neq j \\ 0, & i = j. \end{cases} \quad (14)$$

If the function is symmetric, then the matrix \mathbf{C} is regarded as the weighted adjacency matrix of an undirected graph. Otherwise the graph is directed. We focus only on the undirected case in this article, however directed graphs may also be considered. Note that \mathbf{C} is equivalent to \mathbf{W} in the general case.

We define GVD connectivity as a graph-variate signal analysis with a suitably chosen node space function (6) weighted by a connectivity adjacency matrix, \mathbf{C} , derived from the signal. GVD connectivity then takes the form

$$\theta(\mathbf{x}_i, \mathbf{x}_j, t) = \begin{cases} c_{ij}F_V(x_i(t), x_j(t)), & i \neq j \\ 0, & i = j. \end{cases} \quad (15)$$

By an appropriate choice of F_V this can reveal information of the significance of specific points in time of the connectivity over which the adjacency matrix is constructed. From another perspective, the connectivity adjacency matrix acts as a filter for extracting useful information from the node space function, F_V - strong connectivity implies those vertices are sharing or communicating important information consistently, thus these connections amplify the function at those vertices, whereas weak connectivity implies the opposite and suppresses the function at those vertices [9]. The outline of GVD connectivity is very flexible, but this also means that in its application it requires a carefully considered formulation, as we undertake here, to avoid data-dredging.

A particularly useful analysis for exploring the GVD connectivity associated with a particular node is the *node GVD connectivity*

$$\theta_i(\mathbf{X}, t) = \sum_{j=1}^n c_{ij}F_V(x_i(t), x_j(t)). \quad (16)$$

We will use this a number of times in our experiments. The operator which extracts the vector of node temporal connectivities is defined in (8).

Here we present node functions for three pertinent examples of connectivity adjacency matrices- correlation, coherence and phase-lag index. For clarity of exposition, in each case we will first present the formulae for these connectivity estimates before going on to describe the chosen node space functions to compute GVD connectivity.

A. Correlation

Taking the connectivity estimate as the correlation coefficient we have

$$c_{ij} = \frac{\sum_{t \in T} (x_i(t) - \bar{x}_i)(x_j(t) - \bar{x}_j)}{\sqrt{\sum_{t \in T} (x_i(t) - \bar{x}_i)^2} \sqrt{\sum_{t \in T} (x_j(t) - \bar{x}_j)^2}} \quad (17)$$

where T is the epoch of interest, \bar{x}_i is the mean of the values over time of the node i . In the preliminary formulation, Smith et al. [9] presented GVD connectivity as:

$$\theta(\mathbf{x}_i, \mathbf{x}_j, t) = c_{ij}(\tilde{x}_i(t) - \tilde{x}_j(t))^2, \quad (18)$$

derived from the Dirichlet energy form from GSP [3], where $\tilde{x}_i(t)$ is the normalised signal over the node space, i.e.

$$\tilde{x}_i(t) = \frac{x_i(t) - \bar{x}(t)}{\sqrt{\frac{1}{n-1} \sum_{k=1}^n (x_k(t) - \bar{x}(t))^2}}, \quad (19)$$

where $\bar{x}(t) = \frac{1}{n} \sum_{k=1}^n x_k(t)$ is the mean over vertices of the signal at time t . Notably, the entries of the matrix may be negative which is an important principle, as noted in [9], for maintaining the anti-correlative information. Differences in amplitudes at time t reflect the amplitude dependent correlation coefficient (17). Agreeing terms abide in small instantaneous differences with positive correlation and large instantaneous differences with negative correlation.

From the new framework, we can, however, consider a function deriving more directly from (17):

$$\theta(\mathbf{x}_i, \mathbf{x}_j, t) = c_{ij}|(x_i(t) - \bar{x}_i)(x_j(t) - \bar{x}_j)|, \quad (20)$$

where the node space function here can be understood as a measure of instantaneous correlation coefficient at the time point t . These methods shall be compared in simulations and real data to help reveal the benefits of using more nuanced functions than the classical Dirichlet form.

B. Coherence

The coherence of two channels is a function of frequency, ω , and can be interpreted as a correlation of signal component at ω of the channels. For a chosen frequency band we thus have

$$c_{ij} = \sum_{\omega \in \Omega} \frac{|P_{\mathbf{x}_i \mathbf{x}_j}(\omega)|^2}{P_{\mathbf{x}_i \mathbf{x}_i}(\omega) P_{\mathbf{x}_j \mathbf{x}_j}(\omega)}, \quad (21)$$

where Ω is a frequency band of interest, $P_{\mathbf{x}_i \mathbf{x}_j}$ is the cross-spectral density function of \mathbf{x}_i and \mathbf{x}_j and $P_{\mathbf{x}_i \mathbf{x}_i}$ and $P_{\mathbf{x}_j \mathbf{x}_j}$ the respective power spectral density functions [19].

Similarly as for correlation, we will consider both the squared difference and instantaneous correlations of the instantaneous amplitudes to compute GVD connectivity for

coherence, after bandpassing in the frequency range of interest, i.e.

$$\theta(\mathbf{x}_i, \mathbf{x}_j, t) = c_{ij}(s_i^a(t) - s_j^a(t))^2. \quad (22)$$

and

$$\theta(\mathbf{x}_i, \mathbf{x}_j, t) = c_{ij}|(s_i^a(t) - \bar{s}_i^a)(s_j^a(t) - \bar{s}_j^a)|, \quad (23)$$

respectively. Coherence cannot be negative, thus it is a more straightforward case than correlation- high coherence and large differences in the instantaneous amplitudes can be taken generally as a contrast of information; whereas a small difference in amplitudes implies agreement of information. Thus large GVD connectivity implies some notable epoch of interest in the given time window with the underlying long-term connectivity.

C. Phase-lag index

The Phase-Lag Index (PLI) [20] measures the consistent phase differences between time-series, indicating lead/lag dependencies. As a connectivity estimate, we write

$$c_{ij} = |\langle \text{sgn}(\phi_i(t) - \phi_j(t)) \rangle|, \quad (24)$$

i.e. the magnitude of the average over time of the signed values of differences of the instantaneous phases, $\phi_i(t)$, of the signals.

We choose F_V for phase-based connectivity indexes as the sign of the phase difference of the signals stemming directly from (24), giving

$$\theta(\mathbf{x}_i, \mathbf{x}_j, t) = c_{ij} \text{sgn}(\phi_i(t) - \phi_j(t)). \quad (25)$$

Because of the negative symmetry of this function, the global GVD connectivity of the system at time t is

$$\begin{aligned} \sum_{i,j} \theta(\mathbf{x}_i, \mathbf{x}_j, t) &= \sum_{i < j} (\theta(\mathbf{x}_i, \mathbf{x}_j, t) + \theta(\mathbf{x}_j, \mathbf{x}_i, t)) \\ &= \sum_{i < j} (\theta(\mathbf{x}_i, \mathbf{x}_j, t) - \theta(\mathbf{x}_i, \mathbf{x}_j, t)) = 0. \end{aligned} \quad (26)$$

However, summing over a subset of these elements, for example, only over those edges relating to a given node or subset of nodes, would reveal the strength and general nature of the node(s) to lead (positive) or lag (negative) in the network at the given epoch. In experiments we will apply these GVD connectivity functions to several simulated and real datasets to provide document of their usefulness.

IV. EXPERIMENTS

We now demonstrate these methods in simulations and real data sets. An autoregressive model is implemented first to illustrate the broad idea and benefit of graph-variate signal analysis before we explore the ability of GVD connectivity to correctly discover differences between two large datasets which differ only by the presence (and lack thereof) of a single correlated couple. To test the effectiveness of temporal network clustering coefficient metric (12), we devise a simple regime to detect a spheroid travelling over a 3D grid. We then apply our techniques to real high complexity datasets of geophysical well logs and EEG brain functional connectivity to provide evidence of the benefits delivered by a graph-variate analysis approach.

A. Detecting correlated sources

We generate 5 realisations, 1×1000 vectors $\{\mathbf{z}_i\}_{i=1}^5$, of a stationary autoregressive process with governing equation

$$z(t) = 0.5 + 0.7z(t-1) + 0.25z(t-2) + \epsilon, \quad (27)$$

where $\epsilon \sim \mathcal{N}(0, 0.1)$ and consider the multivariate signal

$$\begin{bmatrix} \mathbf{x}_1 \\ \mathbf{x}_2 \\ \mathbf{x}_3 \end{bmatrix} = \begin{bmatrix} \frac{1}{2} & \frac{1}{2} & 0 & 0 & 0 \\ \frac{1}{2} & 0 & \frac{1}{2} & 0 & 0 \\ 0 & 0 & 0 & \frac{1}{2} & \frac{1}{2} \end{bmatrix} \begin{bmatrix} \mathbf{z}_1 \\ \mathbf{z}_2 \\ \mathbf{z}_3 \\ \mathbf{z}_4 \\ \mathbf{z}_5 \end{bmatrix}, \quad (28)$$

so that all \mathbf{x}_i are the average of two realisations of (27); \mathbf{x}_1 and \mathbf{x}_2 are correlated via the information in \mathbf{z}_2 ; and \mathbf{x}_3 is independent of \mathbf{x}_1 and \mathbf{x}_2 . Fig. 2. A shows the computation of instantaneous correlation coefficients and corresponding node GVD connectivity computed using correlation coefficient (20) over the entire signal. The corresponding graph weights are $w_{12} = 0.6934$, $w_{13} = -0.0576$, $w_{23} = 0.0943$. Node GVD connectivity (bottom) is computed over 5 samples in non-overlapping windows. The corresponding short-term graph weights computed over 5 samples and the un-weighted instantaneous correlation are shown in the 2nd and 3rd plots, respectively. Unsubstantiated dependencies are produced using the short-term graph weight and instantaneous correlation methods where often the three components are roughly equivalent. GVD connectivity, on the other hand suppresses the uncorrelated data using the long-term connectivity estimates and the prevailing information comes forth from the truly correlated data relating to edge (1, 2). This is most obviously seen in comparing instantaneous correlation (third) with GVD connectivity (bottom), where the signals are identical except that GVD connectivity weights them by long-term correlations, hence the yellow, (2, 3), and orange, (1, 3), time-series are suppressed relative to the blue time-series, (1, 2).

We now extend this to quantitatively assess the ability to determine a single couple of correlated signals from increasingly large sets of signals. Following the same autoregressive process as (27), we generate $2 \times h$ realisations for $h = 2, 4, 8, 16, \dots, 512$. Then two sets of signals are formed. The first uncorrelated set takes the average of each consecutive disjoint couple of realisations as the multivariate signal $\mathbf{X} \in \mathbb{R}^{h \times 1000}$. The second set is almost the same except the second signal is formed from the 1st and 4th (rather than 3rd and 4th) realisations so as to be correlated with the first signal. We generate populations of such multivariate signals of sizes 5, 10, 15, \dots , 50 to track effects due to population size. We then compute the difference between the uncorrelated and correlated original signals and GVD connectivity analysis using (18) and (20) and sum over time. We then implement a one-sample t -test on the null hypothesis that the population values have a zero mean with significance indicating rejection of the null hypothesis at the $\alpha = 0.05$ level. The results for each population and signal size are shown in Fig. 3.

The values for the original signals are provided for reference since we do not expect them to perform well given that they rely only on magnitudes. The results clearly indicate that GVD connectivity using instantaneous correlation has greater

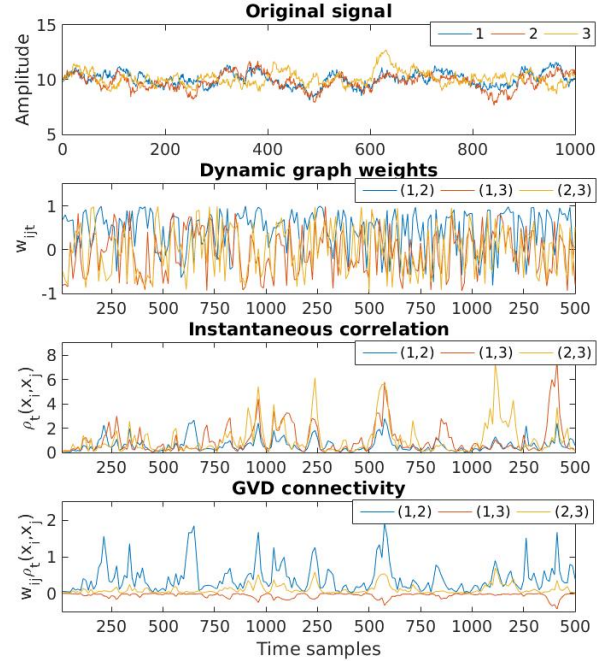


Fig. 2. The original signal (top), dynamic graph weights (second) Instantaneous correlations (third) and corresponding GVD connectivity (bottom) of edges as shown in the legend. The benefit of long-term graph weights is evident, where the GVD connectivity correctly emphasises important information (that related to edge (1,2)).

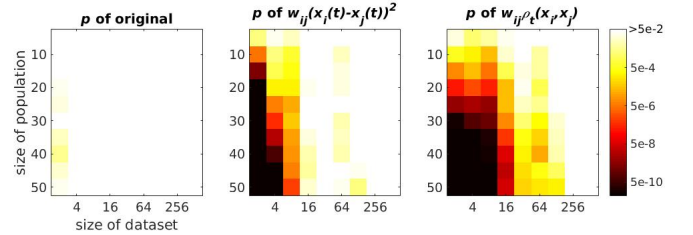


Fig. 3. The p -values of one-sample t -tests of correctly identified correlated sources for different sizes of dataset (x -axis) and population (y -axis) for the original signal (left) and GVD node connectivity with squared difference (middle) and instantaneous correlation (right). White indicates a non-significant difference, black indicates a p -value value smaller than 5×10^{-10} .

sensitivity to differences than using squared difference. Specifically, we can state that GVD connectivity with instantaneous correlation can correctly and reliably identify differences in the AR processes with a population size of 25 or greater with at least 128 signals. Squared difference can detect differences in 128 signals only with a population size of 50. However, even with a population of 50 this is not reliable since it fails to detect the difference in the 32 signal case.

B. Spheroid travelling randomly on a 3D grid

We construct a $10 \times 10 \times 10$ grid in Euclidean space where each point corresponds to a univariate signal. A weighted connectivity graph is formed from the inverse distance, computed as $w_{ij} = \exp(-d_{ij}^2/4)$, between the intersecting points in the grid and amplitudes are distributed normally at random to the vertices as $\mathcal{N}(0, 0.3)$. At time t , the amplitude at node i is increased arbitrarily by an amount, δ , and amplitudes at

those vertices one unit away from i are increased by $\frac{3}{4}\delta$. At time $t + 1$, again amplitudes are assigned normally at random but one of the vertices assigned $\frac{3}{4}\delta$ increased amplitude at time t is now randomly selected for a δ amplitude increase and its closest neighbours are now assigned $\frac{3}{4}\delta$. We can liken this to a spheroid travelling randomly across a grainy image. This process continues for 1000 time steps for values of δ ranging from 0.1 in steps of 0.1 up to 0.9. We now consider the appropriate node space function to use in this scenario. The randomness of movement means that using approaches which try to assess a direction, such as Kalman filtering, are of little value. Thus, a more basic maximisation approach is adopted. Considering that higher amplitudes close together should produce high values, we implement graph-variate signal analyses using a multi-layer graph, Δ , with a node space function which takes the average of each signal pair so that:

$$\Delta_{ijt} = \frac{1}{2}w_{ij}(x_i(t) + x_j(t)). \quad (29)$$

We then calculate the weighted clustering coefficient, C_{loc} , from (12), respectively, at each node at each point in time. The task is then to detect the spheroid at each point in time. We compare with simply choosing the node with highest amplitude and also by implementing graph filtering approaches based on the graph adjacency matrix with self-loops, $\tilde{\mathbf{W}} = \mathbf{I} + \mathbf{W}$ [4], and the graph Laplacian [3], as well as using the heat kernel, $e^{-\tau\mathbf{L}}$ [3]. That is, at time t , we select the highest value of the vectors $\tilde{\mathbf{W}}\mathbf{X}(t)$, $\mathbf{L}\mathbf{X}(t)$, and $e^{-\mathbf{L}}\mathbf{X}(t)$ and also the cubed versions $\tilde{\mathbf{W}}^3\mathbf{X}(t)$, $\mathbf{L}^3\mathbf{X}(t)$, and $e^{-3\mathbf{L}}\mathbf{X}(t)$ to compare a simple GVD connectivity approach with some standard GSP approaches.

We take the largest clustering coefficients as the measure to detect the spheroid at each point in time and compare with just taking the highest amplitude value of the signal and the highest value of the outlined GSP approaches. Fig. 4 details the number of correctly identified spheroid centres (left) and the number of identifications at any point of the spheroid (right), i.e. within one grid square of centre, for each δ . Our approach using C_{loc} (green) achieves best results in 7/9 cases in the former and in all cases in the latter. Our approach shows best overall results in both, see Table I, being one percentage point clear of the next best in detecting the centre and nearly ten percentage points clear of the next best in detecting any part of the spheroid. Of the GSP approaches, the best are the single adjacency matrix filter $\tilde{\mathbf{W}}$ (Fig. 4, dark blue) and the heat kernel $e^{-3\mathbf{L}}$ (orange), which perform relatively well in detecting the centre point. However, they fair much less well when taking into account the sides of the spheroid, where they do not fair much better than the default maximum amplitude approach (black). Since \mathbf{W} and \mathbf{L} fair better than their cubic versions, we know that the improvement noted by the clustering coefficient method is not down to the cube of the graph distance information resulting from (12). Indeed, the graph topology being emphasised in higher powers of the adjacency matrix and graph Laplacian leads to a decrease in the relevant information contained in the signal, which is not dependent on the topology of the grid.

An example of how the proposed method is able to correctly identify a spheroid centre which has been incorrectly identified

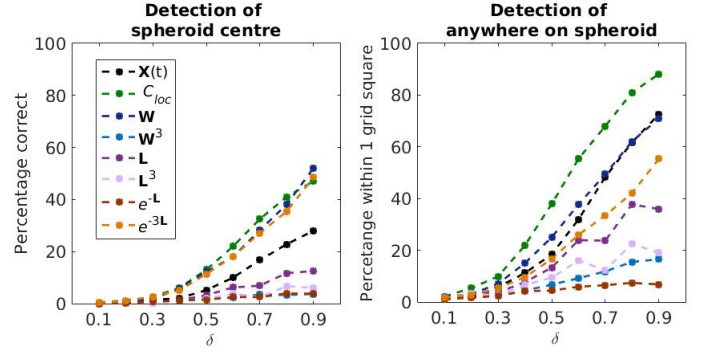


Fig. 4. Total of correct (coloured) and next nearest guesses- 1st to 4th nearest vertices, respectively (stacked, uncoloured)- out of 1000 time points using amplitude height only (max. amp.), signal function graph clustering coefficient, C_{loc} for node functions $(x_i(t) + x_j(t))/2$, C_{loc+} , and $x_i(t)x_j(t)$, $C_{loc\times}$, and graph signal filtering approaches where s is the increased amplitude of the central point of the sphere.

TABLE I
PERCENTAGES (%) FOR DIFFERENT METHODS IN CORRECTLY LOCATING SPHEROID CENTRE (CENTRE) AND IN IDENTIFYING SPHEROID AT ANY POINT (ANY) OVER ALL SIZES OF STRENGTH δ

Locate	max	C_{loc}	$\tilde{\mathbf{W}}$	$\tilde{\mathbf{W}}^3$	\mathbf{L}	\mathbf{L}^3	$e^{-\mathbf{L}}$	$e^{-3\mathbf{L}}$
Centre	9.7	18.4	17.4	1.9	4.8	2.5	1.8	16.6
Any	28.2	41.1	30.3	7.7	16.7	10.3	4.5	21.4

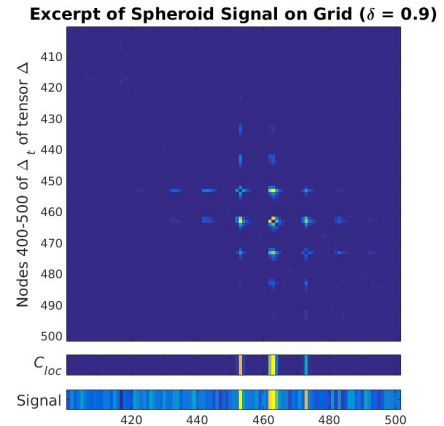


Fig. 5. Example of reduced noise and increased accuracy through clustering coefficient. The highest amplitude is detected at node 452, however the maximum clustering coefficient, C_{loc} , detects the actual centre at node 462.

using the highest amplitude is shown in Fig. 5. In this example, the increased amplitude of $3/4\delta$ given to one of the nearest vertices, 452, provides a larger overall amplitude to the δ given to the central node. By using the graph-variate method, however, this error due to noise is corrected since most of the nearest vertices to 452 have a very small comparative amplitude to those of the true centre at 462.

Analysis of the formulation of the C_{loc} shows its power for the suppression of noise and promotion of clustered phenomena. In the problem illustrated we can consider the

expected value of the signal triple

$$\begin{aligned} E[(x_i + x_j)(x_j + x_k)(x_k + x_i)] &= 8E[x^3] \\ &= 8(\mu_3 + 3E[X]E[X^2] + 2(E[X])^3) \\ &= 8(\mu_3 + 3\mu(\sigma^2 + \mu^2) + 2\mu^3), \end{aligned} \quad (30)$$

where μ is the mean and μ_3 is the third moment of variable x . For only noisy data $x \sim \mathcal{N}(0, \sigma^2)$, this is just zero from the fact that odd moments of a symmetric distribution are zero and $\mu = 0$. On the other hand, the expected value for $x \sim \mathcal{N}(\delta, \sigma^2)$, i.e. data with true value δ in the presence of noise, is $24\sigma^2\delta + 40\delta^3$. For the GSP filtering approaches, the adjacency matrix provides $E[x_i] = 0$ for noise and $E[x_i] = \delta$ for the true value which explains why it also fairs well at detecting the correct centre point, whereas the Laplacian provides $E[x_i - x_j]$ which is zero for noise and true value which explains its poor performance here. We note that this experiment may be too specific to provide a general sense of these approaches, however this highlights the necessity for the appropriate consideration of analysis for the problem at hand which can be assessed more fully within the proposed graph-variate framework. To increase comparability and the pursuit of a simple example, these approaches are chosen to be free from parameters and more complicated methodologies such as using iterative denoising. We recognise, though, that more elaborate complementary methodologies such as implementing wavelets using a dictionary of spheroid shaped atoms [21] or joint time-graph denoising [8] may provide a more intensive treatment of the problem.

C. Gammay ray radiation from well logs

Signals of gamma ray radiation measured in API (American Petroleum Institute) corrected gamma counts across several kilometres (one sample per metre) underground were acquired from well logs in the Kansas Geological survey [22]. Note, these signals are sampled with respect to distance underground (depth) rather than time. Gamma ray radiation is recorded in order to detect shale (indicated by greater Gamma radiation) and is thus useful in oil discovery [23]. As of the 24th of June 2017, data from 23 sites were uploaded of which one was found to be a duplicate of another and one had no gamma ray data. Of the rest, the greatest number, 17, overlapping in depth was found between 2-4km. Large correlation coefficients of these signals indicate similarity in the geology and thus graph-variate analysis should be able to detect substantial changes in geology over large distances in a quick and easy way. We thus compute the correlation coefficient adjacency matrices (17) and compare squared difference (18) and instantaneous correlation (20) in usefulness for the node GVD connectivity of the gamma ray signals.

Fig. 6 shows the results of these versions of GVD connectivity (2nd and 3rd plots, respectively) alongside the original signal (top). Generally, we look for gamma ray counts which are sustained over many tens of metres, indicative of possible reservoirs [23]. Immediate observation of the data shows how GVD connectivity aids manual scrutiny of the signal (left) by dramatically reducing activity particularly for instantaneous correlation, making it easy to spot some immediate epochs and

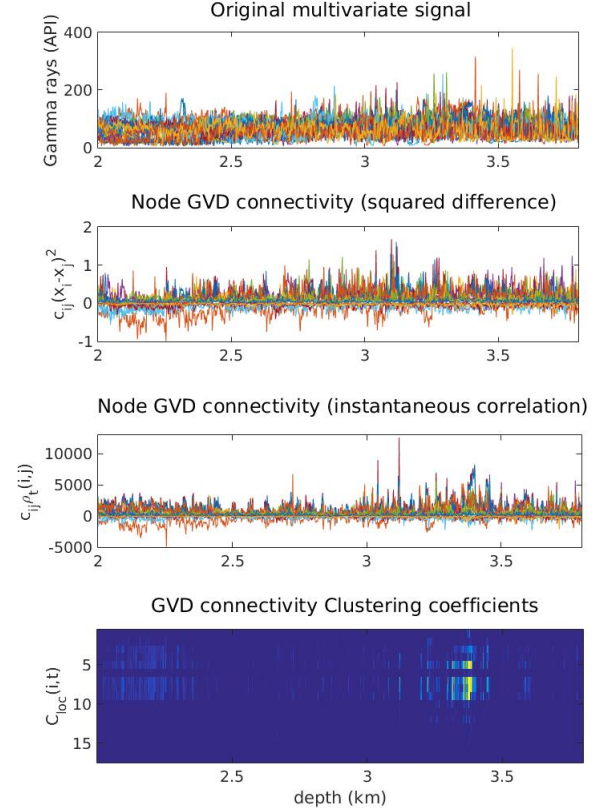


Fig. 6. Seismic data from the June Kansas Geological Survey. Top shows the original gamma ray velocity (American Petroleum Institute (API) units) taken at different points plotted against depth underground (metres). Middle shows the node GVD connectivity using correlation graphs and squared difference. Bottom shows the node GVD connectivity for each node (y -axis) using correlation graphs and instantaneous correlation.

signals of interest. Looking closer at the activity between 3.2-3.5km, there is not much observable activity occurring in the original signal beyond some very short spikes. On the other hand, GVD connectivity with instantaneous correlation clearly shows up very interesting sustained activity occurring in blue, purple and red signals between 3.375-3.4km.

Positive and large activity here suggests that these signals are recorded at similar locations and thus that the related activity indicates a shale component at this depth covering the ground between these sites. Using the graph-variate clustering coefficient (12), this activity clearly sticks out as the most significant correlated activity here (Fig. 6, bottom), where the rest of the activity being sent close to zero indicates uncorrelated and/or noisy data.

D. GVD connectivity of EEG data

We study an eyes-closed, eyes-open dataset of 129-channel EEG activity. This dataset is available online under an open database license from the Neurophysiological Biomarker Toolbox tutorial [24]. It consists of data for 16 volunteers and is down-sampled to 200Hz. We used the clean dataset which we re-referenced to an average reference and filtered in Alpha (8-13Hz) before further analysis. Alpha activity is well known to undergo notable changes between these states [25], thus such

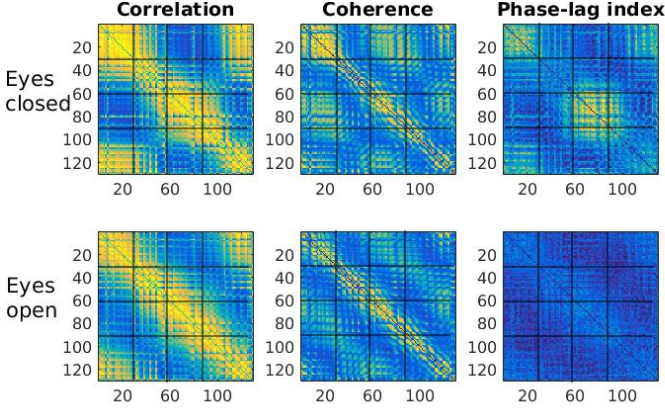


Fig. 7. Weighted graph adjacency matrices of correlation, coherence and PLI for eyes closed (top) and eyes open (bottom) conditions. The colour axes, yellow being the largest weights, are the same for eyes open and eyes closed conditions. Modules are selected based on the most different activity between conditions- Module 1: nodes 1-30, Module 2: nodes 60-90, indicated by the black lines.

a dataset provides a solid testing ground for our techniques on complex brain recordings.

These long recordings- 4.4355 ± 0.2861 mins (mean \pm standard deviation)- allow us to arbitrarily take windows starting at the 1000th sample (5s) to avoid the possibility of pre-processing artefacts at the beginning of the signal. We choose epochs, τ , lasting 16, 32, 64, \dots , 2048 samples (80ms up to 10.24s). We investigate dynamic connectivity using correlation, coherence and PLI in Alpha. For analysis, modules (subsets of nodes) of interest are chosen based on observable differences in the average weights over graphs computed from the largest window- 2048, Fig. 7. Choosing modules, instead of global connectivity, allows us to compute our phase-based methods without redundancy (26). Clearly, around 1-30 nodes and 60-90 nodes show differences in all connectivity measures (Fig. 7, black lines mark 30, 60 and 90), thus we choose these as Module A and Module B, respectively, to compare our methods. Modular connectivity is computed as per the formula in [9]:

$$\sum_{t \in T} \sum_{i \in \mathcal{V}_x} \sum_{j \in \mathcal{V}} c_{ij} F_V(x_i(t), x_j(t)), \quad (31)$$

where \mathcal{V}_x are the module vertices and T is the epoch of interest. Here, i sums over the module and j sums over the entire graph to assess the modules effects on the entire graph. Equation (31) is applied for correlation using (18) and (20), coherence using (22) and (23), and PLI using (25).

For this dataset we seek to clarify the usefulness of our methods compared to weighted graphs by themselves, as implemented in e.g. [14]–[17], as well as the benefit of the graph support in GVD connectivity as opposed to using unweighted node space functions i.e. putting all weights equal 1 in (31). In the latter case, efforts similar to this have been made at determining dynamic connectivity using instantaneous phase differences in fMRI [18].

For modules A and B, we compute GVD connectivity using the pair (T, τ) , where the graph weight is computed over epoch τ and the node function over disjoint epochs of length T , such that $T \leq \tau \in \{16, 32, 64, \dots, 2048\}$. This gives a total

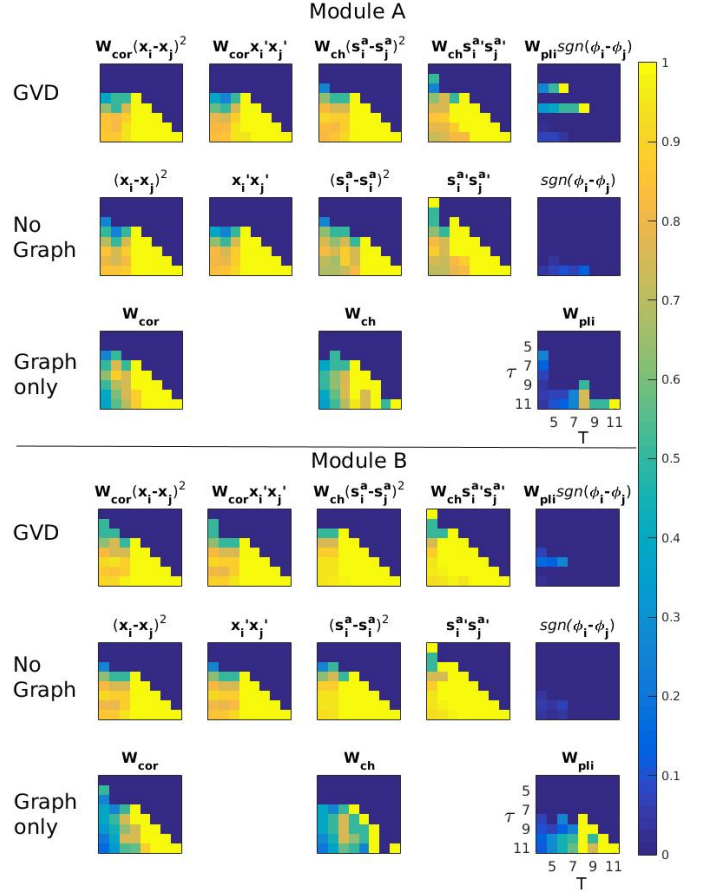


Fig. 8. Results of eyes open vs eyes closed EEG data for Module A, top and Module B, bottom plotted by density of p values which are significant for $T < \tau$. GVD (first row) is GVD connectivity where the graph comes from τ and the GVD is computed over T . The axes of τ against T , shown on the bottom right plot, indicates the signal length considered in powers of 2, i.e. 5 is $2^5 = 32$, etc. No graph (second row) is the non-graph weighted node space function. Graph only (third row) refers to graphs computed over T . \mathbf{W}_{cor} is the adjacency matrix of correlations, \mathbf{W}_{ch} of coherence and \mathbf{W}_{pli} of PLI. Here, \mathbf{x}_i is the original signal, \mathbf{s}_i^a the signal envelope and ϕ_i the instantaneous phase, where \mathbf{x}_i' and $\mathbf{s}_i^{a'}$ are the signals minus their expected values as in (20) and (23), respectively.

of 36 case corresponding to each combination of (T, τ) and a minimum of one p -value (when $T = \tau$) and maximum of $2048/16 = 128$ p -values for these cases. For each (T, τ) we then compute the density, (differences found)/(total possible), of significant p -values found from paired t -tests of eyes closed vs eyes open conditions across the 16 participants. The results for each (T, τ) are shown in Fig. 8 for modules A and B for GVD connectivity, the node functions by themselves (No graph) and a dynamic graph approach (Graph only).

It is clear that for both modules the GVD connectivity approach performs better than the standard dynamic connectivity approach using short-term graphs for correlation and coherence. The phase-lag index fairs poorly in this paradigm in general, but we shall see later that it may be leveraged to greater effect in time-locked task presentation data. It is not clear by observation whether the GVD connectivity approach is better than the node space functions alone (No graph). To see this more evidently, we compute the number of cases,

(T, τ) , for which GVD connectivity outperforms the no graph approach and vice versa, as well as the greater number of significant p -values shown by GVD connectivity within those cases and vice versa. Table II shows the results. We see that GVD connectivity consistently outperforms the node function by itself with a total of 45 cases, consisting of 118 p -values, in which it exceeds the node function alone in module A, and 28 cases, consisting of 50 p -values, in which it exceeds the node function alone in module B. The opposite, in which the node function alone exceeds GVD connectivity is much lower with just 16 cases, consisting of 17 p -values, in module A and 10 cases, consisting of 13 p -values in module B.

TABLE II
NUMBER OF CASES (T, τ) AND p -VALUES WITHIN THOSE CASES (CASES: p -VALUES) FOR WHICH GVD CONNECTIVITY (GVD) FINDS MORE SIGNIFICANT DIFFERENCES ($>$) THAN NODE FUNCTIONS ALONE (NF) AND VICE VERSA. FIRST COLUMN INDICATES GVD METHOD USED (GRAPH/NODE FUNCTION) WHERE COR- CORRELATION, CH- COHERENCE, SQD- SQUARED DIFFERENCE, ICO- INSTANTANEOUS CORRELATION AND PHS- SIGN OF PHASE DIFFERENCE.

Method	Module A		Module B	
	GVD>NF	NF>GVD	GVD>NF	NF>GVD
Cor/sqd	8:16	3:3	10:21	0:0
Cor/ico	4:4	3:3	6:11	0:0
Ch/sqd	14:62	0:0	6:7	1:1
Ch/ico	9:15	6:6	2:2	3:3
PLI/phs	10:21	4:5	4:9	6:9
Total	45:118	16:17	28:50	10:13

To try the PLI in a more appropriate task-related setting where consisting phase dependencies of brain function over many trials can be picked out, we look at a face presentation task, detailed in [26]. The dataset consists of 16 subjects undergoing a face presentation task lasting 1.5 seconds (0.5s pre-stimulus) downsampled from 1kHz to 250Hz. Mean and standard deviation of trials is 294.19 ± 2.32 . After band-passing in Alpha (8-13Hz), the PLI is computed for each trial and then averaged to construct an adjacency matrix per subject. Graph-variate analysis with and without the weighted adjacency matrix is then conducted using sign of instantaneous phase differences. This is conducted per trial, then averaged over trials after which the absolute value is taken. Fig. 9 shows the mean adjacency matrix over subjects ((a) top right) and the resulting C_{loc} for instantaneous phase and GVD connectivity estimates, averaged over subjects. In the GVD connectivity, we can see clearly a strong pattern of dynamic connectivity in nodes 40-60 occurring around 0.3-0.5s after stimulus which dies away and then appears to return again near the 1s mark. This activity occurs after N175 event related potential known to play an important role in face perception tasks [27], suggesting a post N175 phase-based functional response to the visual stimuli. Topoplots confirm that this is more evident using the GVD approach, Fig. 9 (b), where a strong polarity of activity from front right to back left from 0.3-0.5s reoccurring at 0.9-1s is contrasted with a drop in activity from left to back right. Activity from 0.3-0.5s is suggested also in the top left of instantaneous phase only but is less apparent.

As an important aside, these techniques are particularly timely for extending work done on uniting structure and function of the brain as in [28], in which the framework explores

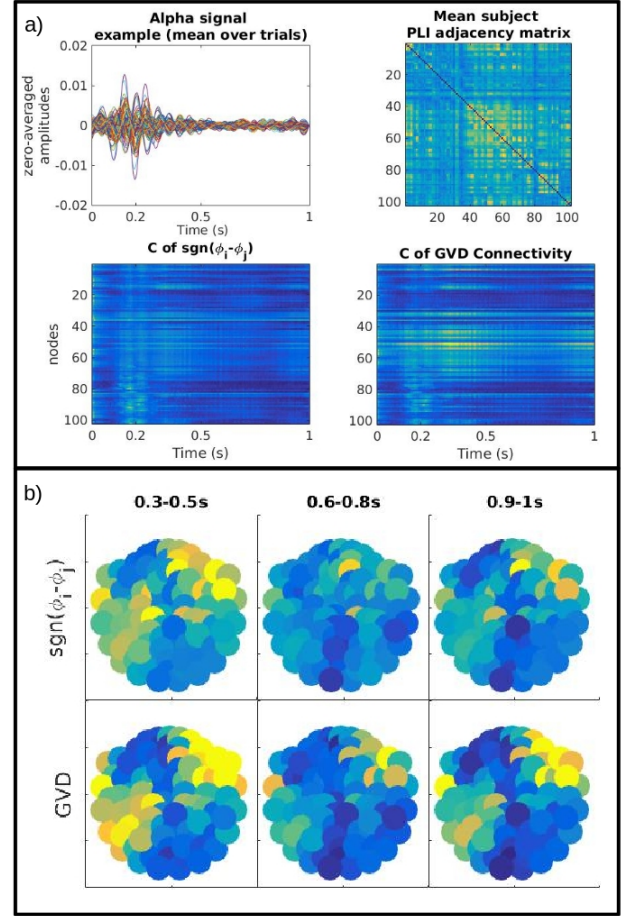


Fig. 9. a) Phase activity from a face presentation task. Top left is the alpha signal for one subject. Top right is the mean connectivity adjacency matrix over all subjects. Bottom left is C_{loc} for each node at each time point for instantaneous PLI, averaged over subjects. Bottom right is C_{loc} for each node at each time point for GVD connectivity, averaged over subjects. b) Topoplots of the sum of C_{loc} phase activity in a given time window from a face presentation task. Colour axis has a minimum (blue) of the 10th and maximum (yellow) of the 90th percentile over all values, time points and subjects. Top is for instantaneous PLI and bottom for GVD connectivity, averaged over subjects.

functional activations over the brain structure but does not yet accommodate for network relationships of synchronously active brain regions, for which graph-variate analysis provides a straightforward solution.

V. CONCLUSION

We defined and provided a general framework for graph-variate signals- unifying frameworks for multivariate signals and graphs. We developed novel analysis of graph-variate signals, considering general graph weighted node space functions. We showed the unique setting occupied by this new form of analysis within the framework, particularly with respect to graph signal processing. We then elaborated on novel methodologies for this analysis towards the temporo-topological analysis of multivariate signals and reliable connectivity estimation at the resolution of the signal. In simulations we showed the robustness of the approach to finding correlations and detecting true activity within large datasets, in the latter instance

outperforming similar state-of-the-art approaches. Pertinently, in differentiating coupling changes between EEG eyes-open and eyes-closed resting states and elucidating instantaneous phase-based activity in a face presentation task, the methods generally outperformed graph only approaches. These methods also show promise in the interpretation and discovery of a wide range of datasets including in geophysics where our techniques can quickly identify areas and epochs of interest in complex datasets. The implications of this theory reach into every domain in which temporal network analysis of multivariate signals is used.

VI. ACKNOWLEDGEMENTS

We would like to thank Phung T.K. Nguyen of the Edinburgh Time-Lapse Project, Heriot-Watt University, for her help in analysing and interpreting the geophysical data from the Kansas Geological Survey. We also thank the editor and reviewers for their considerate feedback.

REFERENCES

- [1] M.E.J. Newman, "Networks", *Oxford University Press*, UK, 2010.
- [2] A.L. Barabási, "Network Science", *Cambridge University Press*, UK, 2016.
- [3] D. Shuman, S.K. Narang, P. Frossard, A. Ortega, P. Vandergheynst, "The emerging field of signal processing on graphs", *IEEE Signal Processing Magazine*, 30(3): 83-98, 2013.
- [4] A. Sandryhaila, J.M.F. Moura, "Discrete signal processing on graphs", *IEEE Transactions on Signal Processing*, 61(7): 1644-1656, 2013.
- [5] A. Sandryhaila, J.M.F. Moura, "Big data analysis with signal processing on graphs: representation and processing of massive data sets with irregular structure", *IEEE Signal Processing Magazine*, 31(5): 80-90, 2014.
- [6] L. Riu, H. Nejati, N-M. Cheung, "Dimensionality reduction of brain imaging data using graph signal processing", *IEEE ICIP Conference 2016*, doi:10.1109/ICIP.2016.7532574, 2016.
- [7] A. Loukas, D. Foucard, "Frequency Analysis of Temporal Graph Signals", *IEEE Global Conference on Signal and Information Processing*, 346-350, 2016.
- [8] F. Grassi, A. Loukas, N. Perraudin, B. Ricaud, "A Time-Vertex Signal Processing Framework", pre-print: arXiv:1705.02307, 2017.
- [9] K. Smith, B. Ricaud, N. Shahid, S. Rhodes, J. Starr, A. Ibanez, M. Parra, J. Escudero, P. Vandergheynst, "Locating Temporal Functional Dynamics in Visual Short Term Memory Tasks using Modular Dirichlet Energy", *Scientific Reports*, 7: 42013, 2017.
- [10] P. Holme, J. Saramäki, "Temporal networks", *Physics reports*, 519(3): 97-125 (2012).
- [11] M. De Domenico, A. Sol-Ribalta, E. Cozzo, M. Kivel, Y. Moreno, M.A. Porter, S. Gmez, and A. Arenas, "Mathematical Formulation of Multilayer Networks", *Phys. Rev. X*, 3: 041022, 2013.
- [12] F.D.V. Fallani, J. Richiardi, M. Chavez, S., Achard, "Graph analysis of functional brain networks: practical issues in translational neuroscience", *Phil. Soc. R. Soc. B*, 369(1653): 20130521, 2014.
- [13] D. Papo, M. Zanin, J.A. Pineda-Pardo, S. Boccaletti, J.M. Buldu, "Functional brain networks: great expectations, hard times and the big leap forward", *Phil. Soc. R. Soc. B*, 369(1653): 20130525, 2014.
- [14] K.W. Doron, D.S. Bassett, M.S. Gazzaniga, "Dynamic network structure of interhemispheric coordination", *PNAS*, 109(46): 18661-18668, 2012.
- [15] N. Leonardi, D. Van De Ville, "On spurious and real fluctuations of dynamic functional connectivity during rest", *NeuroImage*, 104: 430-436, 2015.
- [16] U. Braun, A. Schäfer, H. Walter S. Erk, N. Romanczuk-Seiferth, L. Haddad, J.I. Schweiger, O. Grimm, A. Heinz, H. Tost, A. Meyer-Lindenberg, D.S. Bassett, "Dynamic reconfiguration of frontal brain networks during executive cognition in humans", *PNAS*, 112(37): 11678-11683, 2015.
- [17] U. Braun, A. Schäfer, D.S. Bassett, F. Rausch, J.I. Schweiger, E. Bilek, S. Erk, N. Romanczuk-Seiferth, O. Grimm, L.S. Geiger, L. Haddad, K. Otto, S. Mohnke, A. Heinz, M. Zink, H. Walter, E. Schwarz, A. Meyer-Lindenberg, H. Tost, "Dynamic brain network reconfiguration as a potential schizophrenia genetic risk mechanism modulated by NMDA receptor function", *PNAS*, 113(44): 12568-12573, 2016.
- [18] E. Glerean, J. Salmi, J.M. Lahnakoski, I.P. Jääskelinen, M. Sams, "Functional magnetic resonance imaging phase synchronization as a measure of dynamic functional connectivity", *Brain Connect.*, 20122(2):91-101, 2011.
- [19] T.S. Rappaport, "Wireless communications: principles and practices", *IEEE Press*, ISBN: 0-7803-1167-1, 1996.
- [20] C.J. Stam, G. Nolte, A. Daffertshofer, "Phase lag index: Assessment of functional connectivity from multi channel EEG and MEG with diminished bias from common sources", 28(11): 11781193, 2007.
- [21] D.I. Shuman, C. Wismeyr, N. Holighaus, P. Vandergheynst, "Spectrum-adapted tight graph wavelet and vertex-frequency frames," *IEEE Transactions on Signal Processing*, 63(16):4223-4235, 2015.
- [22] Kansas Geological Survey, gamma ray radiation data acquired from http://www.kgs.ku.edu/PRS/Scans/Log_Summary/index.html, accessed 24th June, 2017.
- [23] M. Rider, M. Kennedy, "The geological interpretation of well logs", 3rd edition, Rider-French Consulting Ltd, Scotland, 2011.
- [24] Neurophysiological Biomarker Toolbox, www.nbtwiki.net, last visited 8th Sept. 2016.
- [25] R.J. Barry, A.R. Clarke, S.J. Johnstone, C.A. Magee, J.A. Rushby, "EEG differences between eyes-closed and eyes-open resting conditions", *Clinical Neurophysiology*, 118(12): 2765-2773, 2007.
- [26] R.N. Henson, D.G. Wakeman, V. Litvak, K.J. Friston (2011), "A parametric empirical Bayesian framework for the EEG/MEG inverse problem: generative models for multi-subject and multi-modal integration", *Frontiers of Human Neuroscience*, 5:76, 2011.
- [27] B. Rossion, S. Caharel, "ERP evidence for the speed of face categorization in the human brain: Disentangling the contribution of low-level visual cues from face perception", *Vision Research*, 51:1297-1311, 2011.
- [28] A. Griffa, B. Ricaud, K. Benzi, X. Bresson, A. Daducci, P. Vandergheynst, J-P. Thiran, P. Hagmann, "Transient networks of spatio-temporal connectivity map communication pathways in brain functional systems", *NeuroImage*, 155:490-502, 2017.